Service Restoration of Distribution System Considering Novel Battery Charging and Swapping Station, Repair Crews, and Network Reconfigurations

Xianqiu Zhao, Qingshan Xu, and Yongbiao Yang

***Abstract*—With the integration of wind power, photovoltaic power, gas turbine, and energy storage, the novel battery charging and swapping station (NBCSS) possesses significant operational flexibility, which can aid in the service restoration of distribution system (DS) during power outages caused by extreme events. This paper presents an integrated optimization model for DS restoration that considers NBCSS, repair crews, and network reconfigurations simultaneously. The objective of this model is to maximize the restored load while minimizing generation costs. To address the uncertainties associated with renewable energies, a two-stage stochastic optimization framework is employed. Additionally, copula theory is also applied to capture the correlation between the output of adjacent renewable energies. The conditional value-at-risk (CVaR) measure is further incorporated into the objective function to account for risk aversion. Subsequently, the proposed optimization model is transformed into a mixed-integer linear programming (MILP) problem. This transformation allows for tractable solutions using commercial solvers such as Gurobi. Finally, case studies are conducted on the modified IEEE 33-bus and 69-bus DSs. The results illustrate that the proposed method not only restores a greater load but also effectively mitigates uncertainty risks.**

***Index Terms*—Novel battery charging and swapping station, distribution system, service restoration, two-stage stochastic optimization, conditional value-at-risk.**

NOMENCLATURE

A. Indices and Sets

Φ_F	Set of lines travelled by crews
Ω_D, Ω_S	Sets of damaged lines and switchable lines
hs	Indices of W_{ij}^U and W_{ij}^D
O_l	Set of potential loops
s	Index of uncertain scenarios
$S_j^{B,d}$	Set of downstream buses connecting to bus j
t, τ	Indices of dispatching period T
W_{ij}^U, W_{ij}^D	Sets of upstream and downstream lines of branch ij

B. Variables

Φ_ρ	Standard multivariate normal distribution
Φ^{-1}	Inverse function of standard normal distribution
$\varepsilon_{ij,t}$	Binary variable indicating whether branch ij is closed at time t
$\beta_{i,c,t}, \alpha_{i,c,t}$	Continuous variables about charging and discharging priorities of batteries
$\delta_{i,c,t}, \theta_{i,c,t}$	Binary variables about charging and discharging priorities of batteries
$\sigma_{c,t}, \sigma_{d,t}$	Binary variables about flag of charging and discharging of charging and discharging equipment (CDE)
$\sigma_{ch,t}, \sigma_{dis,t}$	Binary variables about flag of charging and discharging of energy storage (ES)
$E_{e,t}$	Energy of ES
$f_{i,t}$	Binary variable indicating whether line i is repaired at time t
$N_{i,s,t}$	Quantity of batteries in the i^{th} state of charge (SOC) interval
$N_{i,c,t}, N_{i,d,t}$	Quantities of charging and discharging batteries in the i^{th} SOC interval
$N_{all,c,t}, N_{all,d,t}$	Total quantities of charging and discharging batteries
$P_{all,c,t}, P_{all,d,t}$	Total charging and discharging power of CDE in novel battery charging and swapping station (NBCSS)
$P_{ch,t}, P_{dis,t}$	Charging and discharging power of ES
$P_{g,t}, Q_{g,t}$	Active and reactive power of gas turbine (GT)

Manuscript received: January 2, 2024; revised: March 23, 2024; accepted: March 23, 2024. Date of CrossCheck: April 29, 2024. Date of online publication: June 11, 2024.

This work was funded by the National Natural Science Foundation of China (No. 51936003).

X. Zhao (corresponding author), Q. Xu, and Y. Yang are with School of Electrical Engineering, Southeast University, Nanjing 210096, China, and Q. Xu and Y. Yang are also with Nanjing Center for Applied Mathematics, Nanjing 210096, China (e-mail: xianqiu_zhao@foxmail. com; xuqingshan@seu. edu. cn; 103200017@seu.edu.cn).

DOI: 10.35833/MPCE.2024.000010

$P_t^{\mathrm{N,L}}, Q_t^{\mathrm{N,L}}$ Restored active and reactive power of load in NBCSS

$P_t^{\mathrm{N,WP}}, Q_t^{\mathrm{N,WP}}$ Active and reactive power of wind power (WP) in NBCSS

$P_t^{\mathrm{N,PV}}, Q_t^{\mathrm{N,PV}}$ Active and reactive power of photovoltaic (PV) in NBCSS

$P_{j,t}^{\mathrm{N,ex}}, Q_{j,t}^{\mathrm{N,ex}}$ Exchanged active and reactive power moves from line j to line i

$P_{ij,t}^{\mathrm{D}}, Q_{ij,t}^{\mathrm{D}}$ Active and reactive power flow through branch ij

$P_{j,t}^{\mathrm{D,WP}}, Q_{j,t}^{\mathrm{D,WP}}$ Active and reactive power of WP at bus j

$P_{j,t}^{\mathrm{D,PV}}, Q_{j,t}^{\mathrm{D,PV}}$ Active and reactive power of PV at bus j

$R_{i,c}$ Binary variable indicating whether line i is repaired at time t

$T_{i,c}$ Time when crew c arrives at line i

$V_{i,t}$ Voltage of bus i

$x_{j,i,c}$ Binary variable indicating whether crew c moves from line j to line i

$x_{\mathrm{g},t}, u_{\mathrm{g},t}, v_{\mathrm{g},t}$ Binary variables indicating on/off state of GT

$y_{i,t}$, $y_{k(ij),t}$ Binary variables indicating whether line i and branch ij are available at time t

C. Parameters and Constants

$\lambda_{\mathrm{e,min}}, \lambda_{\mathrm{e,max}}$ The minimum and maximum energy statuses

$\eta_{\mathrm{ch,e}}, \eta_{\mathrm{dis,e}}$ Charging and discharging efficiencies of ES

ε Error factor

Δt Time interval

B_l Number of lines of potential loops

$C^{\mathrm{SU}}, C^{\mathrm{SD}}$ Start-up and shut-down costs of GT

C_{g} Unit generation cost of GT

$E_{\mathrm{e,rate}}$ Rated capacity of ES

K Number of SOC intervals

M_{big} Large number

$N_{\max}$ The maximum quantity of chargers in CDE

$P_{\mathrm{g,min}}, P_{\mathrm{g,max}}$ The minimum and maximum power of GT

$P_{\mathrm{fix,c}}$ Charging power of CDE for a single battery

$P_{\mathrm{fix,d}}$ Discharging power of CDE for a single battery

$P_{\mathrm{ch,max}}$, $P_{\mathrm{dis,max}}$ The maximum charging and discharging of ES

$P_t^{\mathrm{N,L,max}}$, $Q_t^{\mathrm{N,L,max}}$ The maximum active and reactive power of load in NBCSS

$P_{j,t}^{\mathrm{N,ex,max}}$, $Q_{j,t}^{\mathrm{N,ex,max}}$ The maximum exchanged active and reactive power between DS and NBCSS

$P_{j,t}^{\mathrm{D,L,max}}$, $Q_{j,t}^{\mathrm{D,L,max}}$ The maximum active and reactive power of load at bus j

$P_{t,\mathrm{RE}}^{\mathrm{N,WP}}, P_{t,\mathrm{RE}}^{\mathrm{N,PV}}$ The maximum active power of WP and PV in NBCSS

$P_{i,t,\mathrm{RE}}^{\mathrm{D,WP}}, P_{i,t,\mathrm{RE}}^{\mathrm{D,PV}}$ The maximum active power of WP and PV in DS

$r_{ij}^{\mathrm{D}}, x_{ij}^{\mathrm{D}}$ Resistance and reactance of branch ij

$R_{\mathrm{U,g}}, R_{\mathrm{D,g}}$ Ramp-up and ramp-down limits of GT

$S_{\max}^{\mathrm{N,WP}}, S_{\max}^{\mathrm{N,PV}}$ The maximum capacities of WP and PV in NBCSS

$S_{i,\max}^{\mathrm{D,WP}}, S_{i,\max}^{\mathrm{D,PV}}$ The maximum capacities of WP and PV in DS

$S_{\mathrm{g,max}}$ The maximum capacity of GT

$S_{\mathrm{U,g}}, S_{\mathrm{D,g}}$ Start-up and shut-down limits of GT

T Dispatching period

$t_{\mathrm{g}}^{\mathrm{U}}, t_{\mathrm{g}}^{\mathrm{D}}$ The minimum up-time and down-time of GT

t_0 Initial departure time of crews

$t_{j,i,c}^{\mathrm{trip}}$ Travel time between line j and line i of crew c

$t_{j,c}^{\mathrm{rep}}$ Repair time of line j of crew c

$V_{i,\min}, V_{i,\max}$ The minimum and maximum voltage limits of bus i

V_0 Rated voltage magnitude

I. Introduction

In recent years, extreme events such as hurricanes, storms, floods, and cyber-attacks, have caused severe damages to the power grids, resulting in large-scale blackouts and significant economic losses [1]-[3]. For example, in 2019, the super typhoon "Lekima" struck the southeast coast of China, leading to power outages for more than 7 million customers and an economic loss of totaling 53 billion yuan [4]. As a bridge to link the transmission network and customers, the distribution system (DS) is a vital public infrastructure that ensures the normal operation of the social economy. According to the statistics, the failures of DS are responsible for 90% of the customer outage minutes [5]. Consequently, the development of an effective and efficient distribution service restoration (DSR) strategy stands as one of the paramount tasks for utilities.

Numerous studies have examined the service restoration of DS. Among them, network reconfigurations are popularly employed. For instance, a two-stage network reconfiguration method is proposed for the self-healing scheme of DS in [6]. Reference [7] introduces a fully decentralized multi-agent system-based network reconfiguration method for DS, which can lessen the computational burden of service restoration. In [8], an hourly basis network reconfiguration is adopted to enhance the resilience of DS.

Nowadays, the increasing penetration of distributed energy resources (DERs) transforms the operation and control paradigms of DS [9]. In this context, the active DS possesses greater potential for realizing self-healing capability [10]. Photovoltaic (PV) power, wind power (WP), and energy storage (ES) are all considered for the service restoration of DS after wildfire [11]. To cope with the extended events, the adaptive formation of microgrids is proposed for critical service restoration in [12]. Reference [13] presents a sequential

DS service restoration method based on microgrid formation in the case of large-scale power outages. Nevertheless, given the presence of isolated fault regions, complete DS restoration may be impeded until damages are cleared. Hence, some studies have introduced the scheduling of repair crews into the service restoration of DS. Reference [14] proposes a coordinated repair and operation model for the service restoration of DS. In [15], the repair crews, line switch operations, mobile power sources, DERs, and ES are coordinated to maximize the restored load of DS. Reference [16] explores a multi-period coordinated repair scheduling and service restoration for DS, considering soft open points (SOPs). These studies have made substantial contributions to the field of DS restoration, enhancing the feasibility and optimization of the restoration process.

Electric vehicles (EVs) have witnessed widespread adoption across the globe. Battery swapping stations (BSSs), offering the capability to swiftly recharge EVs in mere minutes, have garnered increasing attention. BSS can also play a crucial role in supporting the operation of DS through the flexible process to charge and discharge stocked substantial batteries. Surprisingly, scant research has explored the potential of BSS in service restoration of DS. Reference [17] presents an optimization strategy to improve the resilience of an island microgrid by incorporating BSS in emergency scenarios. Along with network reconfigurations, the BSS is also considered for the service restoration of DS in the case of extreme weather [18]. Reference [19] also proposes a joint service restoration for the DS, where DERs, BBS, and network reconfigurations are included. Nonetheless, these research works come with certain limitations. First, none of them has considered the scheduling of repair crews, whose importance has been highlighted. Furthermore, these research works do not consider the uncertainties of renewable energies, which can significantly impact the restoration process. Additionally, the integration of WP, PV, gas turbine (GT), and ES enables the upgrade of the BSS into a novel battery charging and swapping station (NBCSS), greatly enhancing operational flexibility [20]. The NBCSS holds the potential to further enhance the reliability of service restoration of DS.

The comparison of this paper with the most relevant research works mentioned before is given in Table I. To address the above gaps, this paper proposes a coordination method that integrates crew dispatch with the service restoration of DS while considering the NBCSS. The major contributions of this paper are summarized as follows.

TABLE I
COMPARISON OF THIS PAPER WITH MOST RELEVANT RESEARCH WORKS

Reference	Network reconfiguration	Repair crew	BSS	Uncertainty
[14]	√	√		√
[15]	√	√		√
[16]	√	√		
[17]			√	√
[18]	√		√	
[19]	√		√	
This paper	√	√	√	√

1) An integrated method coordinating NBCSS, repair crews, and network reconfigurations is proposed for the service restoration of DS. The goal of this model is to maximize the restored load while minimizing generation costs.

2) A stochastic optimization framework is employed to cope with the uncertainties of renewable energies, where the potential correlation between the output of adjacent renewable energies is also described by copula theory. Moreover, the conditional value-at-risk (CVaR) measure is included in the objective function for risk aversion.

The rest of the paper is organized as follows. The framework of DS incorporating NBCSS is shown in Section II. Section III gives the model formulation. The two-stage risk-averse stochastic optimization framework is given in Section IV. Case studies are demonstrated in Section V. Finally, Section VI draws the conclusion.

II. FRAMEWORK OF DS INCORPORATING NBCSS

The framework of DS incorporating NBCSS is illustrated in Fig. 1. The DS comprises renewable energies (WP and PV), load, and lines, while the NBCSS is composed of WP, PV, GT, ES, and charging and discharging equipment (CDE). Then, the NBCSS is connected to the DS at a certain node.

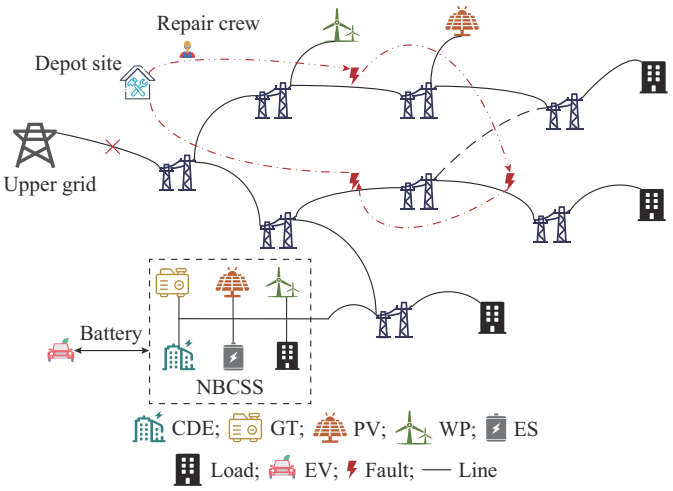

Fig. 1. Framework of DS incorporating NBCSS.

In normal scenarios, the DS can fully meet all load demands, and NBCSS can satisfy all battery requirements. However, during extreme events, the power supply from the upper grid is interrupted, and some distribution lines are damaged, leading to power outages for some users. In such critical situations, the top priority is the service restoration of DS. Before implementing service restoration, fault positioning and assessment are prerequisites. Since this paper focuses on repair and resource scheduling, the locations and repair time of the damages are known from the prerequisites. Hence, with such information, the repair crews are dispatched to repair the damaged lines and restore the outage load, which leave the depot site to repair the damaged lines and return to the depot site once all of the allocated duties have been completed. Meanwhile, the NBCSS suspends its battery swapping services and is arranged to support the load service restoration. In addition, the network configura-

tions are also employed to coordinate the repair crews to reduce the load outage time.

Thus, in this paper, the repair and resource scheduling for DS is co-optimized to minimize the unserved load plus the generation cost by coordinating the NBCSS, repair crews, and network configurations.

III. Model Formulation

A. Model of NBCSS

The state of charge (SOC) interval technique is used to model the batteries in the CDE, as presented in our prior research work [20]. The modeling details can be found in the reference provided and will not be elaborated here.

1) CDE

$$\begin{cases} N_{1,\mathrm{s},t}=N_{1,\mathrm{s},t-1}-N_{1,\mathrm{c},t}+N_{2,\mathrm{d},t} \\ N_{2,\mathrm{s},t}=N_{2,\mathrm{s},t-1}+N_{1,\mathrm{c},t}-N_{2,\mathrm{c},t}-N_{2,\mathrm{d},t}+N_{3,\mathrm{d},t} \\ \vdots \\ N_{K-1,\mathrm{s},t}=N_{K-1,\mathrm{s},t-1}+N_{K-2,\mathrm{c},t}-N_{K-1,\mathrm{c},t}-N_{K-1,\mathrm{d},t}+N_{K,\mathrm{d},t} \\ N_{K,\mathrm{s},t}=N_{K,\mathrm{s},t-1}+N_{K-1,\mathrm{c},t}-N_{K,\mathrm{d},t} \end{cases} \tag{1}$$

$$N_{\mathrm{all,c},t}=\sum_{i=1}^{K-1}N_{i,\mathrm{c},t} \tag{2}$$

$$N_{\mathrm{all,d},t}=\sum_{i=2}^{K}N_{i,\mathrm{d},t} \tag{3}$$

$$\begin{cases} 0\le N_{i,\mathrm{c},t}\le N_{i,\mathrm{s},t-1} \\ 0\le N_{i+1,\mathrm{d},t}\le N_{i+1,\mathrm{s},t-1} \end{cases} \quad i\in 1,2,\ldots,K-1 \tag{4}$$

$$\begin{cases} 0\le N_{\mathrm{all,c},t}\le N_{\max}\sigma_{\mathrm{c},t} \\ 0\le N_{\mathrm{all,d},t}\le N_{\max}\sigma_{\mathrm{d},t} \\ \sigma_{\mathrm{c},t}+\sigma_{\mathrm{d},t}\le 1 \end{cases} \tag{5}$$

$$\begin{cases} 0\le \beta_{i,\mathrm{c},t}-\left(N_{\mathrm{all,c},t}-\sum_{k=1}^{i}N_{K-k,\mathrm{s},t}\right) \\ \beta_{i,\mathrm{c},t}-\left(N_{\mathrm{all,c},t}-\sum_{k=1}^{i}N_{K-k,\mathrm{s},t}\right)\le M_{\mathrm{big}}(1-\delta_{i,\mathrm{c},t}) \\ 0\le \beta_{i,\mathrm{c},t}\le M_{\mathrm{big}}\delta_{i,\mathrm{c},t} \\ N_{K-i,\mathrm{s},t-1}-M_{\mathrm{big}}(1-\delta_{i,\mathrm{c},t})\le N_{K-i,\mathrm{c},t} \\ N_{K-i-1,\mathrm{c},t}\le M_{\mathrm{big}}\delta_{i,\mathrm{c},t} \\ \delta_{i+1,\mathrm{c},t}\le \delta_{i,\mathrm{c},t} \end{cases} \quad i\in 1,2,\ldots,K-2 \tag{6}$$

$$\begin{cases} 0\le \alpha_{i,\mathrm{c},t}-\left(N_{\mathrm{all,d},t}-\sum_{k=1}^{i}N_{k+1,\mathrm{s},t}\right) \\ \alpha_{i,\mathrm{c},t}-\left(N_{\mathrm{all,d},t}-\sum_{k=1}^{i}N_{k+1,\mathrm{s},t}\right)\le M_{\mathrm{big}}(1-\theta_{i,\mathrm{c},t}) \\ 0\le \alpha_{i,\mathrm{c},t}\le M_{\mathrm{big}}\theta_{i,\mathrm{c},t} \\ N_{i+1,\mathrm{s},t-1}-M_{\mathrm{big}}(1-\theta_{i,\mathrm{c},t})\le N_{i+1,\mathrm{d},t} \\ N_{i+2,\mathrm{d},t}\le M_{\mathrm{big}}\theta_{i,\mathrm{c},t} \\ \theta_{i+1,\mathrm{c},t}\le \theta_{i,\mathrm{c},t} \end{cases} \quad i\in 1,2,\ldots,K-2 \tag{7}$$

$$\begin{cases} P_{\mathrm{all,c},t}=N_{\mathrm{all,c},t}P_{\mathrm{fix,c}} \\ P_{\mathrm{all,d},t}=N_{\mathrm{all,d},t}P_{\mathrm{fix,d}} \end{cases} \tag{8}$$

Equation (1) gives the quantitative relationship of batteries for different SOC intervals. The limitations on the overall amounts of charging and discharging batteries are given in (2) and (3). The restrictions on the amount of charging and discharging batteries, which are determined by the SOC intervals, are presented in (4). Equation (5) gives mutually exclusive limitations for charging and discharging batteries. Equations (6) and (7) demonstrate the charging and discharging priorities determined by the big-*M* method. Equation (8) states the total power of charging and discharging batteries.

2) GT

$$x_{\mathrm{g},t}-x_{\mathrm{g},t-1}=u_{\mathrm{g},t}-v_{\mathrm{g},t} \tag{9}$$

$$u_{\mathrm{g},t}+v_{\mathrm{g},t}\le 1 \tag{10}$$

$$u_{\mathrm{g},t}\le x_{\mathrm{g},\tau}\quad \forall t\le\tau\le t+t_{\mathrm{g}}^{\mathrm{U}}-1 \tag{11}$$

$$v_{\mathrm{g},t}\le 1-x_{\mathrm{g},\tau}\quad \forall t\le\tau\le t+t_{\mathrm{g}}^{\mathrm{D}}-1 \tag{12}$$

$$P_{\mathrm{g,min}}x_{\mathrm{g},t}\le P_{\mathrm{g},t}\le P_{\mathrm{g,max}}x_{\mathrm{g},t} \tag{13}$$

$$-S_{\mathrm{g,max}}x_{\mathrm{g},t}\le Q_{\mathrm{g},t}\le S_{\mathrm{g,max}}x_{\mathrm{g},t} \tag{14}$$

$$P_{\mathrm{g},t}-P_{\mathrm{g},t-1}\le R_{\mathrm{U,g}}x_{\mathrm{g},t-1}\Delta t+S_{\mathrm{U,g}}u_{\mathrm{g},t}\Delta t \tag{15}$$

$$P_{\mathrm{g},t-1}-P_{\mathrm{g},t}\le R_{\mathrm{D,g}}x_{\mathrm{g},t}\Delta t+S_{\mathrm{D,g}}v_{\mathrm{g},t}\Delta t \tag{16}$$

$$P_{\mathrm{g},t}^2+Q_{\mathrm{g},t}^2\le S_{\mathrm{g,max}}^2 \tag{17}$$

Equations (9) and (10) express the start-up and shut-down relationships. Equations (11) and (12) present the minimum up-time and down-time restrictions. The active and reactive power constraints are ensured in (13) and (14), while the ramp-up and ramp-down restrictions are given in (15) and (16). Equation (17) shows that the active power and reactive power are restricted by the maximum capacity of apparent power.

3) ES

$$E_{\mathrm{e},t}=\begin{cases} E_{\mathrm{e},0} & t=0 \\ E_{\mathrm{e},t-1}+\left(\eta_{\mathrm{ch,e}}P_{\mathrm{ch},t}-\dfrac{P_{\mathrm{dis},t}}{\eta_{\mathrm{dis,e}}}\right)\Delta t & t\ge 1 \end{cases} \tag{18}$$

$$\lambda_{\mathrm{e,min}}E_{\mathrm{e,rate}}\le E_{\mathrm{e},t}\le\lambda_{\mathrm{e,max}}E_{\mathrm{e,rate}} \tag{19}$$

$$E_{\mathrm{e},T}=E_{\mathrm{e},0} \tag{20}$$

$$0\le P_{\mathrm{ch},t}\le P_{\mathrm{ch,max}}\sigma_{\mathrm{ch},t} \tag{21}$$

$$0\le P_{\mathrm{dis},t}\le P_{\mathrm{dis,max}}\sigma_{\mathrm{dis},t} \tag{22}$$

$$\sigma_{\mathrm{ch},t}+\sigma_{\mathrm{dis},t}\le 1 \tag{23}$$

Equations (18)-(20) illustrate the energy constraints of ES, while (21)-(23) specify the constraints of charging and discharging power of ES.

4) Restored Load

$$0\le P_t^{\mathrm{N,L}}\le P_t^{\mathrm{N,L,max}} \tag{24}$$

$$0\le Q_t^{\mathrm{N,L}}\le Q_t^{\mathrm{N,max}} \tag{25}$$

$$Q_t^{\mathrm{N,L,max}}P_t^{\mathrm{N,L}}=Q_t^{\mathrm{N,L}}P_t^{\mathrm{N,L,max}} \tag{26}$$

Equations (24) and (25) give the limits of restored load. Equation (26) demonstrates a fixed ratio between restored active and reactive power.

5) Renewable Energies

1) WP

$$0 \le P_t^{\mathrm{N,WP}} \le P_{t,\mathrm{RE}}^{\mathrm{N,WP}} \tag{27}$$

$$(P_t^{\mathrm{N,WP}})^2 + (Q_t^{\mathrm{N,WP}})^2 \le (S_{\max}^{\mathrm{N,WP}})^2 \tag{28}$$

2) PV

$$0 \le P_t^{\mathrm{N,PV}} \le P_{t,\mathrm{RE}}^{\mathrm{N,PV}} \tag{29}$$

$$(P_t^{\mathrm{N,PV}})^2 + (Q_t^{\mathrm{N,PV}})^2 \le (S_{\max}^{\mathrm{N,PV}})^2 \tag{30}$$

Equations (27) and (29) show that the active power output of renewable energies is limited by the maximum available value. Equations (28) and (30) indicate that the active power and reactive power are restricted by the maximum capacity of apparent power.

6) Exchanging Power

$$P_{j,t}^{\mathrm{N,ex}} = P_{\mathrm{g},t} + P_{\mathrm{dis},t} - P_{\mathrm{ch},t} + P_t^{\mathrm{N,WP}} + P_t^{\mathrm{N,PV}} - P_t^{\mathrm{N,L}} + P_{\mathrm{all,d},t} - P_{\mathrm{all,c},t} \tag{31}$$

$$Q_{j,t}^{\mathrm{N,ex}} = Q_{\mathrm{g},t} + Q_t^{\mathrm{N,WP}} + Q_t^{\mathrm{N,PV}} - Q_t^{\mathrm{N,L}} \tag{32}$$

$$-P_{j,t}^{\mathrm{N,ex,max}} \le P_{j,t}^{\mathrm{N,ex}} \le P_{j,t}^{\mathrm{N,ex,max}} \tag{33}$$

$$-Q_{j,t}^{\mathrm{N,ex,max}} \le Q_{j,t}^{\mathrm{N,ex}} \le Q_{j,t}^{\mathrm{N,ex,max}} \tag{34}$$

Equations (31) and (32) give the active and reactive power of NBCSS exchanged with DS. Equations (33) and (34) give the maximum limits of exchanged active and reactive power.

B. Scheduling of Repair Crews

The optimal scheduling of repair crews can be modeled by using the graph theory [21]. Its goal is to seek the best route for each repair crew to reach the damaged components. Assume there are N damaged lines in an extreme event and define the node set of damaged lines Φ_F as $\{1, 2, \ldots, N\}$ with the depot node as $\{0\}$. Then, the route table, which is $N+1$ dimension square matrix composed of binary entries, is employed to properly portray the crew routing alternative. Each repair crew leaves from depot node 0 to repair damaged lines and ultimately returns to the depot node 0. Figure 2 illustrates the crew route decision and its associated route table value. The constraints related to the crew route decision are presented as below.

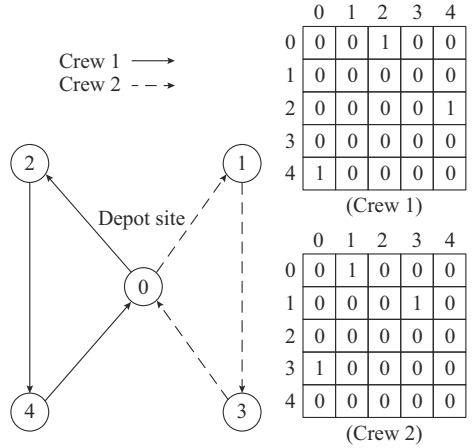

	0	1	2	3	4
0	0	0	1	0	0
1	0	0	0	0	0
2	0	0	0	0	1
3	0	0	0	0	0
4	1	0	0	0	0

(Crew 1)

	0	1	2	3	4
0	0	1	0	0	0
1	0	0	0	1	0
2	0	0	0	0	0
3	1	0	0	0	0
4	0	0	0	0	0

(Crew 2)

Fig. 2. Illustration of crew route decision and its associated route table value.

$$\sum_{i \in \Phi_{\mathrm{F}}} x_{0,i,c} = 1 \quad \forall c \tag{35}$$

$$\sum_{i \in \Phi_{\mathrm{F}}} x_{i,0,c} = 1 \quad \forall c \tag{36}$$

$$\sum_{j \in \Phi_{\mathrm{F}}} x_{j,i,c} - \sum_{k \in \Phi_{\mathrm{F}}} x_{i,k,c} = 0 \quad \forall c, \forall i \tag{37}$$

$$R_{i,c} = \sum_{j \in \Phi_{\mathrm{F}}} x_{j,i,c} \quad \forall c, \forall i \tag{38}$$

$$\sum_{c} R_{i,c} = 1 \quad \forall i \tag{39}$$

$$T_{0,c} = t_0 \quad \forall c \tag{40}$$

$$T_{i,c} - T_{0,c} \le t_{0,i,c}^{\mathrm{trip}} + M_{\mathrm{big}}(1 - x_{j,i,c}) \quad \forall c \tag{41}$$

$$t_{0,i,c}^{\mathrm{trip}} - M_{\mathrm{big}}(1 - x_{0,i,c}) \le T_{i,c} - T_{0,c} \quad \forall c \tag{42}$$

$$T_{i,c} - T_{j,c} \le t_{j,i,c}^{\mathrm{trip}} + t_{j,c}^{\mathrm{rep}} + M_{\mathrm{big}}(1 - x_{j,i,c}) \quad \forall c, \forall i,j \in \Phi_{\mathrm{F}} \tag{43}$$

$$t_{j,i,c}^{\mathrm{trip}} + t_{j,c}^{\mathrm{rep}} - M_{\mathrm{big}}(1 - x_{j,i,c}) \le T_{i,c} - T_{j,c} \quad \forall c, \forall i,j \in \Phi_{\mathrm{F}} \tag{44}$$

$$0 \le T_{i,c} \le M_{\mathrm{big}} R_{i,c} \quad \forall i \in \Phi_{\mathrm{F}} \tag{45}$$

$$\sum_{t} f_{i,t} = 1 \quad \forall i \in \Phi_{\mathrm{F}} \tag{46}$$

$$\sum_{t} t f_{i,t} \le \sum_{c} (T_{i,c} + t_{j,c}^{\mathrm{rep}} R_{i,c}) + 1 - \varepsilon \quad \forall i \in \Phi_{\mathrm{F}} \tag{47}$$

$$\sum_{c} (T_{i,c} + t_{j,c}^{\mathrm{rep}} R_{i,c}) \le \sum_{t} t f_{i,t} \quad \forall i \in \Phi_{\mathrm{F}} \tag{48}$$

$$y_{i,t} \le \sum_{\tau=1}^{t-1} f_{i,\tau} \quad \forall i \in \Phi_{\mathrm{F}} \tag{49}$$

Equations (35) and (36) enforce that each crew starts and ends its routes at depot node 0. Equation (37) implies that each crew repairs the damaged lines sequentially. Equations (38) and (39) assume that each damaged line is repaired by only one crew and only once. Equation (40) gives the time when each repair crew leaves the depot node. Equations (41) and (42) present the relationship between the arrival time at damaged line i and the departure time from the depot node. Equations (43) and (44) also imply the relationship of arrival time between damaged lines i and j. Equation (45) limits the value of the arrival time of each crew. Equations (46)-(48) calculate the repair completion time of damaged lines i. Equation (49) gives the relationship between the repair state and the available state of damaged line i. It means that the damaged lines are available right away once they are fixed.

C. Fault Isolation and Network Reconfigurations

When a line is damaged, fault isolation is required to ensure the normal operation of the remaining parts [22]. Moreover, network reconfigurations are also used to improve the operational flexibility of DS. The relevant constraints are given as:

$$\varepsilon_{ij,t} = 1 \quad \forall (i,j) \notin \{\Omega_{\mathrm{D}} \bigcup \Omega_{\mathrm{S}}\} \tag{50}$$

$$\varepsilon_{ij,t} \le y_{k(ij),t} \quad \forall i, \forall j \tag{51}$$

$$\varepsilon_{hs,t} \le y_{k(ij),t} \quad \forall i, \forall j, \forall (h,s) \in W_{ij}^{\mathrm{U}} \bigcup W_{ij}^{\mathrm{D}} \tag{52}$$

$$\sum_{(i,j)\in B_l}\varepsilon_{ij,t}\le B_l-1\quad\forall l\in O_l \tag{53}$$

Equation (50) defines the default status of the nondamaged and nonswitchable lines. Equation (51) shows that the switch state of the damaged lines is restricted by the corresponding available state. Equation (52) achieves fault isolation by restricting the switch state of the upstream and downstream switches. Equation (53) is the radiality constraint, which ensures that each potential loop in the DS has at least one line open.

D. Model of DS

The linearized DistFlow branch model is used to model the DS [23].

$$P_{j,t}^{\mathrm{N,ex}}+P_{j,t}^{\mathrm{D,WP}}+P_{j,t}^{\mathrm{D,PV}}+P_{ij,t}^{\mathrm{D}}=\sum_{k\in S_j^{B,d}}P_{jk,t}^{\mathrm{D}}+P_{j,t}^{\mathrm{D,L}} \tag{54}$$

$$Q_{j,t}^{\mathrm{N,ex}}+Q_{j,t}^{\mathrm{D,WP}}+Q_{j,t}^{\mathrm{D,PV}}+Q_{ij,t}^{\mathrm{D}}=\sum_{k\in S_j^{B,d}}Q_{jk,t}^{\mathrm{D}}+Q_{j,t}^{\mathrm{D,L}} \tag{55}$$

$$V_{i,t}-V_{j,t}\le(P_{ij,t}^{\mathrm{D}}r_{ij}^{\mathrm{D}}+Q_{ij,t}^{\mathrm{D}}x_{ij}^{\mathrm{D}})/V_0+M_{\mathrm{big}}(1-\varepsilon_{ij,t}) \tag{56}$$

$$(P_{ij,t}^{\mathrm{D}}r_{ij}^{\mathrm{D}}+Q_{ij,t}^{\mathrm{D}}x_{ij}^{\mathrm{D}})/V_0-M_{\mathrm{big}}(1-\varepsilon_{ij,t})\le V_{i,t}-V_{j,t} \tag{57}$$

$$V_{i,\min}\le V_{i,t}\le V_{i,\max} \tag{58}$$

$$-P_{ij,t}^{\mathrm{D,max}}\varepsilon_{ij,t}\le P_{ij,t}^{\mathrm{D}}\le P_{ij,t}^{\mathrm{D,max}}\varepsilon_{ij,t} \tag{59}$$

$$-Q_{ij,t}^{\mathrm{D,max}}\varepsilon_{ij,t}\le Q_{ij,t}^{\mathrm{D}}\le Q_{ij,t}^{\mathrm{D,max}}\varepsilon_{ij,t} \tag{60}$$

$$0\le P_{j,t}^{\mathrm{D,L}}\le P_{j,t}^{\mathrm{D,L,max}} \tag{61}$$

$$0\le Q_{j,t}^{\mathrm{D,L}}\le Q_{j,t}^{\mathrm{D,L,max}} \tag{62}$$

$$Q_{j,t}^{\mathrm{D,L,max}}P_{j,t}^{\mathrm{D,L}}=P_{j,t}^{\mathrm{D,L,max}}Q_{j,t}^{\mathrm{D,L}} \tag{63}$$

$$0\le P_{i,t}^{\mathrm{D,WP}}\le P_{i,t,\mathrm{RE}}^{\mathrm{D,WP}} \tag{64}$$

$$(P_{i,t}^{\mathrm{D,WP}})^2+(Q_{i,t}^{\mathrm{D,WP}})^2\le(S_{i,\max}^{\mathrm{D,WP}})^2 \tag{65}$$

$$0\le P_{i,t}^{\mathrm{D,PV}}\le P_{i,t,\mathrm{RE}}^{\mathrm{D,PV}} \tag{66}$$

$$(P_{i,t}^{\mathrm{D,PV}})^2+(Q_{i,t}^{\mathrm{D,PV}})^2\le(S_{i,\max}^{\mathrm{D,PV}})^2 \tag{67}$$

Equations (54) and (55) represent the nodal balance constraints of active and reactive power. Equations (56) and (57) show the relationship between the magnitude of nodal voltage and the flow of branch power. Equation (58) sets the limits on nodal voltage magnitudes. Equations (59) and (60) show that branch power flows are restricted by their capacities and switch states. Equations (61) and (62) give the limits of restored power at node j. Equation (63) demonstrates a fixed ratio between restored active and reactive power at bus j. Similarly, (64)-(67) give the constraints of the active and reactive power of renewable energies in the DS.

E. Objective Function

The objective function is expressed by (68)-(70). We define that f_1 is the total priority-weighted energy not served; f_2 is the start-up, shut-down, and generation costs of GT; ω_j and ω_{N} are the load weights; and λ_1 and λ_2 are the weighting factors used to link the two sub-objective functions. In order not to encumber the load restoration, λ_1 is set to be bigger than λ_2.

$$f=\min\{\lambda_1 f_1+\lambda_2 f_2\} \tag{68}$$

$$f_1=\sum_t\left[\sum_i\omega_j(P_{j,t}^{\mathrm{D,L,max}}-P_{j,t}^{\mathrm{D,L}})+\omega_{\mathrm{N}}(P_t^{\mathrm{N,max}}-P_t^{\mathrm{N,L}})\right] \tag{69}$$

$$f_2=\sum_t(C^{\mathrm{SU}}u_{\mathrm{g},t}+C^{\mathrm{SD}}v_{\mathrm{g},t}+C_{\mathrm{g}}P_{\mathrm{g},t}) \tag{70}$$

IV. Two-stage Risk-averse Stochastic Optimization Framework

A. Copula-based Correlation Description

The copula function is utilized to characterize the correlation between the output of adjacent renewable energies (e.g., WP and PV). It can effectively capture the relationship between the marginal distribution and joint distribution of random variables.

As stated by Sklar's theorem [24], any joint cumulative distribution function $F(X_1,X_2,\ldots,X_M)$ can be expressed as marginal distribution functions $\{F_1(X_1),F_2(X_2),\ldots,F_M(X_M)\}$ and a copula function $C(\cdot)$, as shown in (71).

$$F(X_1,X_2,\ldots,X_M)=C(F_1(X_1),F_2(X_2),\ldots,F_M(X_M)) \tag{71}$$

Differentiating (71), the joint probability distribution function $f(X_1,X_2,\ldots,X_M)$ can be obtained as:

$$f(X_1,X_2,\ldots,X_M)=c(F_1(X_1),F_2(X_2),\ldots,F_M(X_M))\prod_{i=1}^{M}f_i(X_i) \tag{72}$$

where $f_i(X_i)$ is the probability density function of function $F_i(X_i)$; and $c(F_1(X_1),F_2(X_2),\ldots,F_M(X_M))$ is the copula density function as:

$$c(F_1(X_1),F_2(X_2),\ldots,F_M(X_M))=\frac{\partial C(F_1(X_1),F_2(X_2),\ldots,F_M(X_M))}{\partial(F_1(X_1))\partial(F_2(X_2))\ldots\partial(F_M(X_M))} \tag{73}$$

Various copula functions such as Gaussian Copula, Gumbel Copula, and Frank Copula have been constructed to reveal the dependence of uncertain variables. In this paper, the multivariate Gaussian copula function is utilized to explore the correlation, as expressed in (74).

$$C_{\mathrm{Gau}}=\Phi_\rho(\Phi^{-1}(F_1(X_1)),\Phi^{-1}(F_2(X_2)),\ldots,\Phi^{-1}(F_M(X_M))) \tag{74}$$

With the multivariate Gaussian copula function, we can generate the corresponding scenarios where the correlation is considered.

B. Two-stage Stochastic Optimization

In this subsection, we adopt the two-stage stochastic optimization method to cope with the uncertainties of renewable energies. First, according to the probability distribution and correlation of prediction error, the copula-based method mentioned above is used to generate a large number of random scenarios. Then, the scenario reduction method such as K-medoids clustering is applied to select representative scenarios for lessening the calculative burden [25]. For N_s representative scenarios, the corresponding objective function is presented below with φ_s as the probability of the s^{th} scenario.

$$\min\sum_s\varphi_s(\lambda_1 f_{1,s}+\lambda_2 f_{2,s}) \tag{75}$$

$$f_{1,s}=\sum_{t}\left[\sum_{i}\omega_j\left(P_{j,t}^{\mathrm{D,L,max}}-P_{j,t,s}^{\mathrm{D,L}}\right)+\omega_{\mathrm{N}}\left(P_{t}^{\mathrm{N,max}}-P_{t,s}^{\mathrm{N,L}}\right)\right] \tag{76}$$

$$f_{2,s}=\sum_{t}\left(C^{\mathrm{SU}}u_{\mathrm{g},t}+C^{\mathrm{SD}}v_{\mathrm{g},t}+C_{\mathrm{g}}P_{\mathrm{g},t,s}\right) \tag{77}$$

Similarly, the corresponding constraints need to be updated. Considering the content redundancy, they are omitted.

Note that $\boldsymbol{x}$ is the first-stage variable; $\boldsymbol{u}_s$ is the value of scenario s; $\boldsymbol{y}_s$ is the second-stage variables in scenario s; and $\boldsymbol{A}$, $\boldsymbol{B}$, $\boldsymbol{C}$, $\boldsymbol{D}$, $\boldsymbol{b}$, $\boldsymbol{c}$, $\boldsymbol{d}$ and $\boldsymbol{e}$ are the corresponding matrixes and vectors. The mode is recasted as the compact matrix form as below. The definitions of all variables can be found in [20].

$$\min_{\boldsymbol{x}}\left\{\boldsymbol{c}^{\mathrm{T}}\boldsymbol{x}+\sum_{s\in N_s}\varphi_s\boldsymbol{d}^{\mathrm{T}}\boldsymbol{y}_s\right\} \tag{78}$$

s.t.

$$\boldsymbol{A}\boldsymbol{x}\le\boldsymbol{b} \tag{79}$$

$$\boldsymbol{B}\boldsymbol{x}+\boldsymbol{C}\boldsymbol{y}_s+\boldsymbol{D}\boldsymbol{u}_s\le\boldsymbol{e}\quad\forall s \tag{80}$$

$$\begin{aligned}\boldsymbol{x}=[&N_{\mathrm{new},t},N_{\mathrm{i,s},t},N_{\mathrm{all,c},t},P_{\mathrm{all,c},t},\delta_{\mathrm{i,c},t},\beta_{i,\mathrm{c},t},N_{\mathrm{all,d},t},P_{\mathrm{all,d},t},\sigma_{\mathrm{c},t},\sigma_{\mathrm{d},t},\\&\alpha_{i,\mathrm{c},t},\theta_{\mathrm{i,c},t},u_{\mathrm{g},t},v_{\mathrm{g},t},x_{\mathrm{g},t},x_{i,j,c},R_{i,c},T_{i,c},f_{i,t},y_{i,t},\varepsilon_{ij,t}]\end{aligned} \tag{81}$$

$$\boldsymbol{u}_s=[P_{i,t,s,\mathrm{RE}}^{\mathrm{D,WP}},P_{i,t,s,\mathrm{RE}}^{\mathrm{D,PV}},P_{t,s,\mathrm{RE}}^{\mathrm{N,WP}},P_{t,s,\mathrm{RE}}^{\mathrm{N,PV}}] \tag{82}$$

$$\begin{aligned}\boldsymbol{y}_s=\{&P_{\mathrm{g},t,s},P_{t,s}^{\mathrm{N,WP}},Q_{t,s}^{\mathrm{N,WP}},P_{t,s}^{\mathrm{N,PV}},Q_{t,s}^{\mathrm{N,PV}},P_{t,s}^{\mathrm{N,L}},Q_{t,s}^{\mathrm{N,L}},E_{\mathrm{e},t,s},\\&P_{\mathrm{ch},t,s},P_{\mathrm{dis},t,s},\sigma_{\mathrm{ch},t,s},\sigma_{\mathrm{dis},t,s},P_{j,t,s}^{\mathrm{NBCSS}},Q_{j,t,s}^{\mathrm{NBCSS}},P_{ij,t,s}^{\mathrm{D}},Q_{ij,t,s}^{\mathrm{D}},\\&P_{j,t,s}^{\mathrm{D,WP}},Q_{j,t,s}^{\mathrm{D,WP}},P_{j,t,s}^{\mathrm{D,PV}},Q_{j,t,s}^{\mathrm{D,PV}},P_{j,t,s}^{\mathrm{D,L}},Q_{j,t,s}^{\mathrm{D,L}},V_{i,t,s}\}\end{aligned} \tag{83}$$

C. Risk Management

The optimal solution $\boldsymbol{x}^*$ is derived based on the optimization problem (78)-(83). Its goal is to minimize the expectation of all representative scenarios, presenting a risk-neutral style. This means the results may be optimistic and lead to excessive losses in some unfavorable scenarios. For some operators, they are risk averse and do not want to bear too much loss. Therefore, to manage the risk brought by uncertainties, the CVaR index [26] is the utilized in this paper, as expressed by (84). Note that ζ is value-at-risk (VaR); α is the confidential level; f_s is the loss function of scenario s; and $[\cdot]^+=\max\{0,\cdot\}$.

$$CVaR=\min_{\zeta,f_s}\left\{\zeta+\frac{1}{1-\alpha}\sum_{s\in N_s}\varphi_s[f_s-\zeta]^+\right\} \tag{84}$$

With CVaR considered, the objective function is modified as follows. Note that ρ_s is an auxiliary variable; and κ is the weighting factor of CVaR.

$$\min_{\boldsymbol{x}}\left\{\boldsymbol{c}^{\mathrm{T}}\boldsymbol{x}+\sum_{s\in N_s}\varphi_s\boldsymbol{d}^{\mathrm{T}}\boldsymbol{y}_s+\kappa\left(\zeta+\frac{1}{1-\alpha}\sum_{s\in N_s}\varphi_s\rho_s\right)\right\} \tag{85}$$

$$\rho_s\ge\boldsymbol{d}^{\mathrm{T}}\boldsymbol{y}_s-\zeta \tag{86}$$

$$\rho_s\ge0 \tag{87}$$

Two linear inequalities are introduced to replace the nonlinear term $[f_s-\zeta]^+$.

D. Linear Approximation

To improve the solving efficiency, the linear approximation method is adopted to replace the quadratic constraints of (17), (28), (30), (65), and (67), which is prevalent in engineering applications [27].

$$\begin{cases}P_{\mathrm{g},t}+Q_{\mathrm{g},t}\le\sqrt{2}\,S_{\mathrm{g,max}}\\P_{\mathrm{g},t}-Q_{\mathrm{g},t}\le\sqrt{2}\,S_{\mathrm{g,max}}\end{cases} \tag{88}$$

$$\begin{cases}P_{t}^{\mathrm{N,WP}}+Q_{t}^{\mathrm{N,WP}}\le\sqrt{2}\,S_{\max}^{\mathrm{N,WP}}\\P_{t}^{\mathrm{N,WP}}+Q_{t}^{\mathrm{N,WP}}\le\sqrt{2}\,S_{\max}^{\mathrm{N,WP}}\\-S_{\max}^{\mathrm{N,WP}}\le Q_{t}^{\mathrm{N,WP}}\le S_{\max}^{\mathrm{N,WP}}\end{cases} \tag{89}$$

$$\begin{cases}P_{t}^{\mathrm{N,PV}}+Q_{t}^{\mathrm{N,PV}}\le\sqrt{2}\,S_{\max}^{\mathrm{N,PV}}\\P_{t}^{\mathrm{N,PV}}-Q_{t}^{\mathrm{N,PV}}\le\sqrt{2}\,S_{\max}^{\mathrm{N,PV}}\\-S_{\max}^{\mathrm{N,PV}}\le Q_{t}^{\mathrm{N,PV}}\le S_{\max}^{\mathrm{N,PV}}\end{cases} \tag{90}$$

$$\begin{cases}P_{i,t}^{\mathrm{D,WP}}+Q_{i,t}^{\mathrm{D,WP}}\le\sqrt{2}\,S_{i,\max}^{\mathrm{D,WP}}\\P_{i,t}^{\mathrm{D,WP}}-Q_{i,t}^{\mathrm{D,WP}}\le\sqrt{2}\,S_{i,\max}^{\mathrm{D,WP}}\\-S_{i,\max}^{\mathrm{D,WP}}\le Q_{i,t}^{\mathrm{D,WP}}\le S_{i,\max}^{\mathrm{D,WP}}\end{cases} \tag{91}$$

$$\begin{cases}P_{i,t}^{\mathrm{D,PV}}+Q_{i,t}^{\mathrm{D,PV}}\le\sqrt{2}\,S_{i,\max}^{\mathrm{D,PV}}\\P_{i,t}^{\mathrm{D,PV}}-Q_{i,t}^{\mathrm{D,PV}}\le\sqrt{2}\,S_{i,\max}^{\mathrm{D,PV}}\\-S_{i,\max}^{\mathrm{D,PV}}\le Q_{i,t}^{\mathrm{D,PV}}\le S_{i,\max}^{\mathrm{D,PV}}\end{cases} \tag{92}$$

In summary, the original problem is transformed into a mixed-integer linear programming, which can be tractably solved by off-the-shelf solvers such as Gurobi.

V. Case Studies

In this section, case studies are employed to test the effectiveness and performance of the proposed method. The optimization problem is solved using the GUROBI solver utilizing MATLAB and YALMIP.

A. System Parameters

The modified IEEE 33-bus DS [28] is used to verify the proposed method. The topology structure of modified IEEE 33-bus DS is shown in Fig. 3. The test system includes three remote-controlled switches on lines 12-22, 18-33, and 25-29. The NBCSS connects to the test system via bus 10. Additionally, two PVs are installed on buses 15 and 28, and a WP is installed on bus 5. T is set to be 24 hours with Δt equaling 1 hour. During an extreme event, six lines (L1-L6) are damaged, and the DS is disconnected from the upper grid, as shown in Fig. 3. There is only one depot site in the DS. Then, two repair crews are arranged to repair the damaged lines. The repair time of the damaged lines is listed in Table II. The travel time between damaged lines ranges from 0 to 1 hour. The main system parameters are shown in Table III, where SOC_0 - SOC_7 are defined by [20]. Critical load in DS is located at buses 4, 10, 13, 21, 24 and 27. They should be prioritized for power supply. Hence, the weight of the critical load is set to be 3, and the weight of the normal load is set to be 1. Figure 4 gives the day-ahead predicted power of WP, PV, and load in DS and NBCSS. Figure 5 depicts the

initial number of batteries categorized by different SOC intervals in the NCBSS. To account for the uncertainties of renewable energies, the standard deviation of WP and PV is set to be 15% and 20% of their mean value, respectively. Additionally, both WPs and PVs have their correlation coefficients set at 0.8. Then, 1000 scenarios are first generated and reduced to 10 representative ones using the *K*-medoids clustering method. In the objective function, weighting factors λ_1 and λ_2 are set to be 1 and 0.8, respectively. With risk aversion considered, κ and α are set to be 1 and 0.9, respectively.

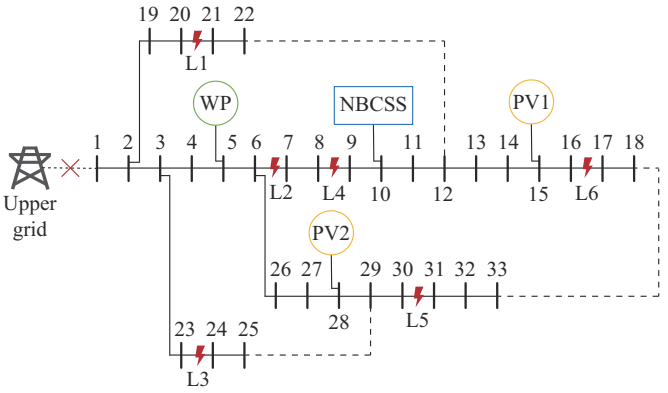

Fig. 3. Topology structure of modified IEEE 33-bus DS.

TABLE II
REPAIR TIME OF DAMAGED LINES

Crew	Repair time (hour)					
	L1	L2	L3	L4	L5	L6
Crew 1	3	4	3	4	3	3
Crew 2	3	3	4	3	4	3

TABLE III
SYSTEM PARAMETERS

Parameter	Value	Parameter	Value
$P_{g,min}$	500 kW	C^{SD}	¥70
$P_{g,max}$	2000 kW	C_g	0.9 ¥/kWh
t_g^U	4 hour	$V_{i,min}^D$	0.93
t_g^D	4 hour	$V_{i,max}^D$	1.07
$R_{U,g}$	1000 kW	V_0^D	1
$R_{D,g}$	1000 kW	K	7
$S_{U,g}$	1000 kW	N_{all}	700
$S_{D,g}$	1000 kW	N_{max}	300
$\eta_{ch,e}$	0.93	$P_{fix,c}$	5 kW
$\eta_{dis,e}$	0.92	$P_{fix,d}$	4.5 kW
$P_{ch,max}$	1000 kW	$[SOC_0, SOC_1]$	[0.2, 0.3]
$P_{dis,max}$	1000 kW	$[SOC_1, SOC_2]$	[0.3, 0.4]
$E_{e,0}$	1500 kWh	$[SOC_2, SOC_3]$	[0.4, 0.5]
$E_{e,rate}$	3000 kWh	$[SOC_3, SOC_4]$	[0.5, 0.6]
$\lambda_{e,min}$	0.2	$[SOC_4, SOC_5]$	[0.6, 0.7]
$\lambda_{e,max}$	0.9	$[SOC_5, SOC_6]$	[0.7, 0.8]
C^{SU}	¥60	$[SOC_6, SOC_7]$	[0.8, 0.9]

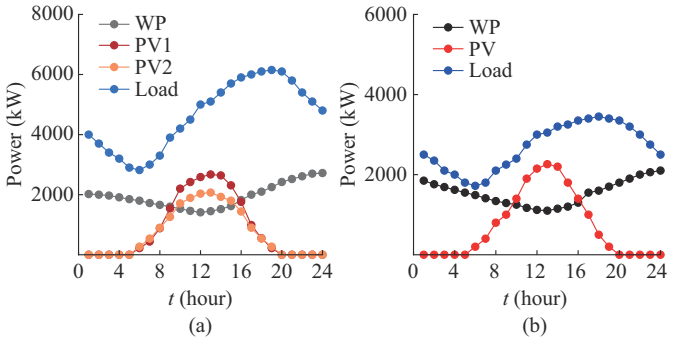

Fig. 4. Day-ahead predicted power of WP, PV and load in DS and NBCSS. (a) DS. (b) NBCSS.

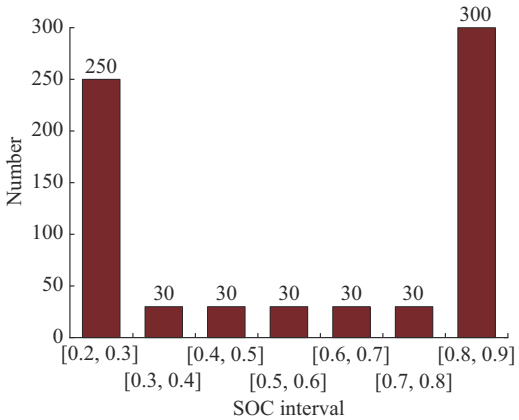

Fig. 5. Initial number of batteries with different SOC intervals.

B. Optimization Results

The routes of repair crews are shown in Fig. 6.

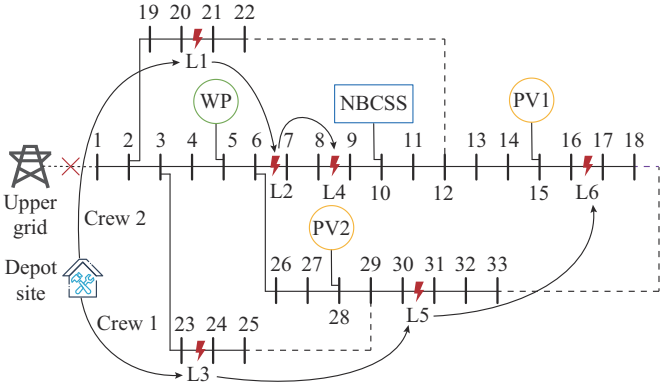

Fig. 6. Routes of repair crews.

Crew 1 is first dispatched from the depot site to the damaged line L3, and then L5 and L6. Crew 2 is first dispatched from the depot site to damaged line L1 and then L2 and L4. Since the critical load at buses 21 and 24 is affected by damaged lines L1 and L3, the crews repair them preferentially. The repair completion and available time of damaged lines are also given in Table IV. Corresponding to the repair routes, the repair completion time of damaged lines L1 and L3 is the shortest (both are 3.5 hours). The two lines can be available at hour 5. The repair completion time of damaged

lines L2 and L5 is 6.8 hours and 7.1 hours, respectively. They can be available at hour 8 and hour 9, respectively. The damaged lines L4 and L6 are repaired at hour 10 and hour 10.6, respectively. Then, all damaged lines can be repaired at hour 12.

TABLE IV
REPAIR COMPLETION AND AVAILABLE TIME OF DAMAGED LINES

Damaged line	Repair completion time (hour)	Available time (hour)
L1	3.5	5
L2	6.8	8
L3	3.5	5
L4	10.0	11
L5	7.1	9
L6	10.6	12

The status of remote-controlled switches are presented in Table V. From hour 1 to hour 4, the switch 12-22 is closed to supply power for the load at bus 22. From hour 5 to hour 24, all switches are closed to reconfigure the system. Additionally, isolated microgrids can be formed to restore the load. For example, Fig. 7 gives the topology of microgrid formulation at hour 1. After faults occur, two microgrids are formed with the help of remote-controlled switches. Microgrid 1 is responsible for supplying power to the load at buses 2, 3, 4, 5, and 19. Microgrid 2 is responsible for supplying power to the load at buses 10, 11, 12, 13, 14, 15, and 22.

TABLE V
STATUSES OF REMOTE-CONTROLLED SWITCHES

Time	Status of remote-controlled switch		
	12-22	18-33	25-29
Hour 1 to hour 4	1	0	0
Hour 5 to hour 24	1	1	1

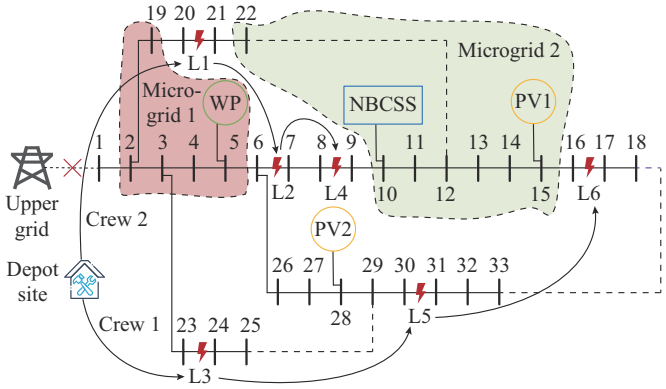

Fig. 7. Topology of microgrid formulation.

The operation status of GT in NBCSS is shown in Fig. 8. During the periods of hour 1 to hour 15, the GT is turned off. Then, the GT is turned on to supply the insufficient power at hour 16 to hour 24. The power of CDE in NBCSS is also presented in Fig. 9. It is primarily charged during the periods of hour 6 to hour 13 and discharged during the periods of hour 1 to hour 5 and hour 16 to hour 24. Therefore, the mismatch between the load and renewable energies can be reduced.

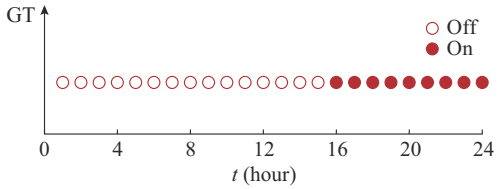

Fig. 8. Operation status of GT in NBCSS.

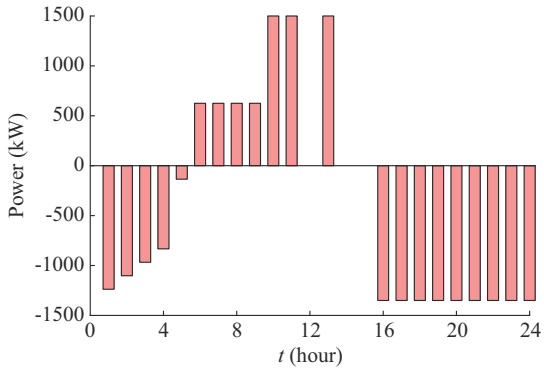

Fig. 9. Power of CDE in NBCSS.

Moreover, Fig. 10 also presents the optimal results in the second stage for one of the possible scenarios. Corresponding to the operation status, GT generates electricity during the periods of hour 16 to hour 24. Besides, the NBCSS provides power for DS during the periods of hour 1 to hour 5 and hour 16 to hour 24. By contrast, the surplus power generated by renewable energies is absorbed by the NBCSS during the periods of hour 6 to hour 15. The NBCSS helps the DS to restore more load and reduce the curtailment of renewable energies.

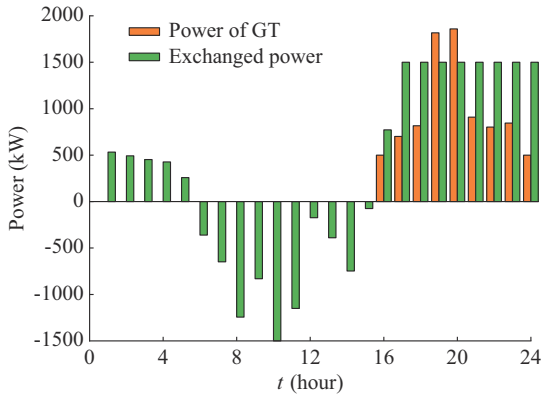

Fig. 10. Optimal results in the second stage.

C. Impact of Network Reconfigurations, NBCSS, and BSS

The impact of network reconfigurations, NBCSS, and BSS on service restoration is analyzed in the next four cases. Case 1 is the proposed method. Case 2 does not consider the network reconfiguration, while case 3 does not consider

the NBCSS. Case 4 only considers the BSS. The total restored load of DS is shown in Table VI. It can be observed that the total restored load of the proposed method is the biggest. Meanwhile, the total restored load of case 3 is much less than that of case 2. It demonstrates that the NBCSS has a greater impact on service restoration than network reconfiguration. Compared with case 3, the total restored load of case 4 has been greatly increased with the help of BSS. However, its total restored load is not as high as case 1. It proves that the operational flexibility of NBCSS is greater than that of BSS. Besides, the restored load at different time is also given in Fig. 11. Before all the damaged lines are repaired, some load can be restored with the assistance of network reconfiguration. Therefore, the restored load of case 1 is more than that of case 2 during hour 1 to hour 12. After all the damaged lines are repaired, case 1 and case 2 have the same restored load, while case 4 has a lower restored load. Moreover, without the support of NBCSS or BSS, the restored load of case 3 is particularly less than that of case 1, case 2, and case 4 during the periods of hour 15 to hour 24. This underscores the effective service restoration achieved through the coordination of network reconfiguration and NBCSS.

TABLE VI
TOTAL RESTORED LOAD OVER ALL TIME PERIODS

Case	Total restored load (kWh)
Case 1	85059
Case 2	83482
Case 3	69929
Case 4	82298

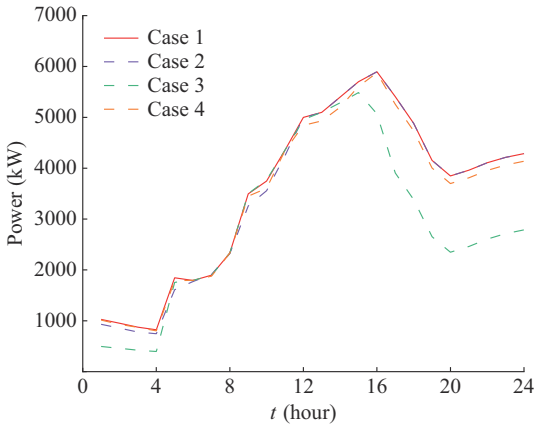

Fig. 11. Restored load at different time.

D. Comparison with Deterministic Optimization

Out-of-sample analyses are used to compare the performance of the proposed method and deterministic optimization. The deterministic optimization, as detailed in section III, completely ignores the prediction error. The day-ahead optimization results are first obtained based on the corresponding methods. Following this, the entire optimization problem is solved using 1000 new out-of-sample scenarios based on the day-ahead results. The computational performance for the two methods is summarized in Table VII. In terms of both the average and worst-case values of the total restored load, the proposed method consistently outperforms deterministic optimization. This outcome emphasizes the necessity of fully accounting for uncertainties related to renewable energies.

TABLE VII
COMPUTATIONAL PERFORMANCE FOR TWO METHODS

Method	Total restored load (kWh)	
	Average value	Worst-case value
Proposed method	84417	77308
Deterministic optimization	83935	76184

E. Impact of Initial Capacity of Stocked Batteries

The initial capacity of stocked batteries in NBCSS is influenced by EV behavior. In this subsection, we delve into the impact of the initial capacity of stocked batteries on service restoration. According to the number of initial batteries with different SOCs in NBCSS, the initial capacity ratio can be easily calculated. Consequently, three different initial capacity ratios (0.3, 0.5, and 0.8) are designated for comparative analysis, representing low, medium, and high initial capacity ratios, respectively. The total restored load and generation cost under different ratios are listed in Table VIII. Notably, the total restored load remains largely consistent across the three ratios. However, there is a reduction in generation cost as the initial capacity ratio increases. This is mainly attributed to the GT in NBCSS, which can provide insufficient power, making the NBCSS more effective in supporting the service restoration of DS.

TABLE VIII
TOTAL RESTORED LOAD AND GENERATION COST UNDER DIFFERENT RATIOS

Initial capacity ratio	Total restored load (kWh)	Generation cost (¥)
0.3	85019	11353
0.5	85049	9027
0.8	85065	8065

F. Sensitivity Analysis on Number of Stochastic Scenarios

In this subsection, the sensitivity analysis is carried out to evaluate the impact of the number of stochastic scenarios on the optimization results. In addition to the 10 typical scenarios reduced from 1000 scenarios, 5, 15, and 20 typical scenarios are utilized for comparison. The comparison results of different numbers of stochastic scenarios are listed in Table IX. As the number of stochastic scenarios increases, the objective function value converges to ¥77671, accompanied by a gradual rise in computation time. Particularly, the objective function values vary much between stochastic scenario 5 and stochastic scenario 10. By comparison, the objective function values vary little between stochastic scenario 10 and stochastic scenario 20. These findings suggest that utilizing 10 typical scenarios strikes a balance between result accuracy and solution time.

TABLE IX
COMPARISON RESULTS OF DIFFERENT NUMBERS OF STOCHASTIC SCENARIOS

Number of stochastic scenarios	Objective function value (¥)	Solution time (s)
5	75275	512
10	77042	932
15	77393	1613
20	77671	4123

G. Computation Complexity Analysis on Number of Damaged Lines

The repair crew routing is a NP-hard problem, significantly amplifying the computational complexity of the proposed method. The more the number of damaged lines, the greater the computational complexity. Therefore, the solution time with different numbers of damaged lines is discussed, as shown in Table X. With the increase in the number of damaged lines, the solution time increases in a more than linear manner. Consequently, when dealing with a substantial number of damaged lines, certain measures such as pre-assignment of repair tasks [16], must be taken to alleviate computation time.

TABLE X
SOLUTION TIME WITH DIFFERENT NUMBER OF DAMAGED LINES

Number of damaged lines	Solution time (s)
3	323
6	932
9	2362

H. Test on Modified IEEE 69-bus DS

As depicted in Fig. 12, the modified IEEE 69-bus DS [29] is also simulated to further verify the proposed method. The NBCSS links to the DS by bus 8. One WP and two PVs are also placed in the DS. Besides, the DS possesses three remote-controlled switches. There are nine damaged lines in the DS. Three repair crews in two depot sites are responsible for repairing damaged lines. To accelerate the solution time, the repair crews 1 and 2 are arranged for damaged lines L1-L6, while the repair crew 3 is arranged for damaged lines L7-L9. The repair time of the nine damaged lines is listed in Table XI.

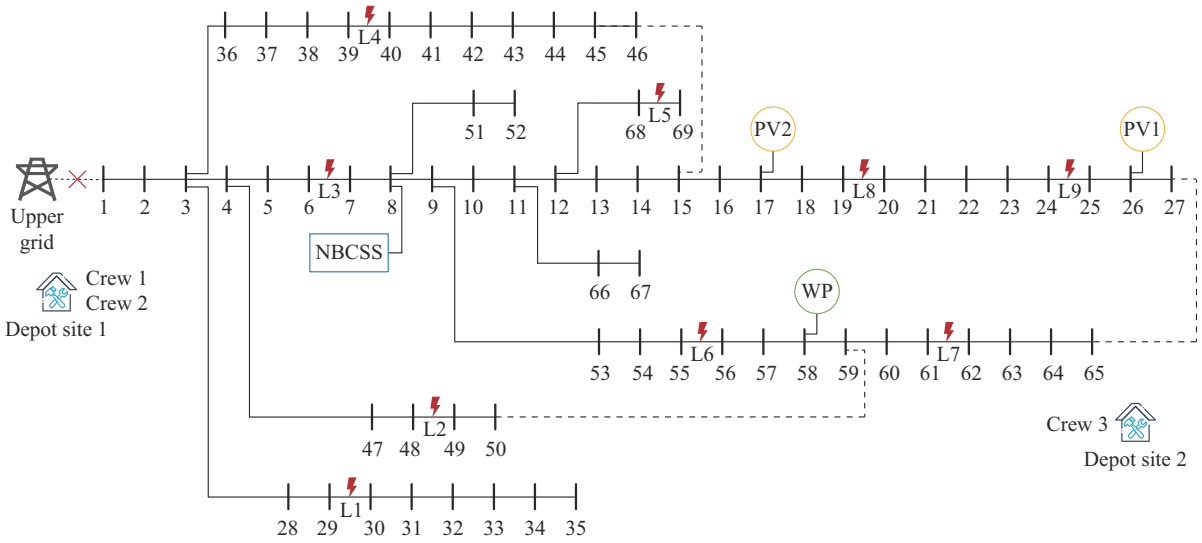

Fig. 12. Topology structure of modified IEEE 69-bus DS.

TABLE XI
REPAIR TIME OF DAMAGED LINES FOR THREE CREWS

Crew	Repair time (hour)								
	L1	L2	L3	L4	L5	L6	L7	L8	L9
Crew 1	3	3	3	4	3	4			
Crew 2	3	4	3	3	3	4			
Crew 3							3	3	4

Under the given relevant parameters, the optimization problem is successfully solved. Table XII presents the routing of different repair crews, while Table XIII presents repair completion and available time of damaged lines. Besides, the restored load of DS at different time is also given in Fig. 13. As the damaged lines are sequentially repaired, the load of the DS gradually recovers. The results verify the effectiveness of the proposed method again.

TABLE XII
ROUTING OF DIFFERENT REPAIR CREWS

Crew	Sequence of repair
Crew 1	Depot site 1→L2→L1→L6→Depot site 1
Crew 2	Depot site 1→L4→L3→L5→Depot site 1
Crew 3	Depot site 2→L7→L8→L9→Depot site 2

VI. CONCLUSION

This paper proposes service restoration considering NBCSS, repair crews, and network reconfigurations.

TABLE XIII
REPAIR COMPLETION AND AVAILABLE TIME OF NINE DAMAGED LINES

Damaged line	Repair completion time (hour)	Available time (hour)
L1	6.7	8
L2	3.5	5
L3	6.9	8
L4	3.6	5
L5	10.2	12
L6	11.1	13
L7	3.5	5
L8	6.8	8
L9	11.1	13

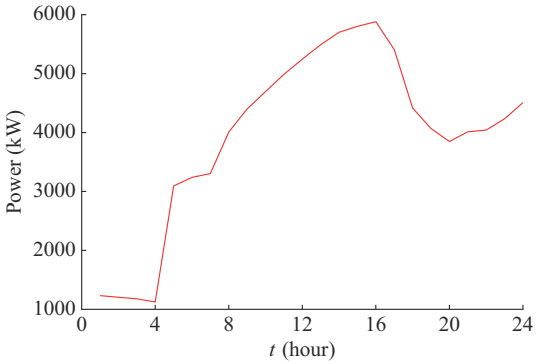

Fig. 13. Restored load of DS at different time.

Furthermore, the stochastic optimization is employed to cope with the uncertainties of renewable energies, while CVaR measure is also considered for risk aversion. In the stochastic optimization model, copula theory is further adopted to capture the correlation between the output of adjacent renewable energies. The results of case studies indicate that the proposed method can effectively dispatch crews to repair damaged lines and NBCSS to support the DS. Besides, the coordination of the NBCSS, repair crews, and network reconfigurations can restore more load than no coordination at all. Moreover, the uncertainty risks of renewable energies are well addressed.

In this paper, the movement of repair crews is assumed to be within a normal transportation system. However, extreme events have a destructive impact on the transportation system. In future work, we will integrate the transportation system into the service restoration problem of DS.

REFERENCES

[1] Z. Ye, C. Chen, B. Chen *et al*., "Resilient service restoration for unbalanced distribution systems with distributed energy resources by leveraging mobile generators," *IEEE Transactions on Industrial Informatics*, vol. 17, no. 2, pp. 1386-1396, Feb. 2021.

[2] Z. Wang, T. Ding, C. Mu *et al*., "A distributionally robust resilience enhancement model for transmission and distribution coordinated system using mobile energy storage and unmanned aerial vehicle," *International Journal of Electrical Power & Energy Systems*, vol. 152, pp. 109256-109256, Oct. 2023.

[3] M. Tian, Z. Dong, L. Gong *et al*., "Coordinated repair crew dispatch problem for cyber-physical distribution system," *IEEE Transactions on Smart Grid*, vol. 14, no. 3, pp. 2288-2300, May 2023.

[4] Y. Zhang, H. Wu, F. Zhang *et al*., "Influence of typhoon on modern smart grid in China and suggested countermeasures," in *Proceedings of Chinese Automation Congress*, Shanghai, China, Nov. 2020, pp. 1-10.

[5] A. H. Alobaidi, S. S. Fazlhashemi, M. Khodayar *et al*., "Distribution service restoration with renewable energy sources: a review," *IEEE Transactions on Sustainable Energy*, vol. 14, no. 2, pp. 1151-1168, Apr. 2023.

[6] P. L. Cavalcante, J. C. López, J. F. Franco *et al*., "Centralized self-healing scheme for electrical distribution systems," *IEEE Transactions on Smart Grid*, vol. 7, no. 1, pp. 145-155, Jan. 2016.

[7] W. Li, Y. Li, C. Chen *et al*., "A full decentralized multi-agent service restoration for distribution network with DGs," *IEEE Transactions on Smart Grid*, vol. 11, no. 2, pp. 1100-1111, Mar. 2020.

[8] E. Kianmehr, S. Nikkhah, V. Vahidinasab *et al*., "A resilience-based architecture for joint distributed energy resources allocation and hourly network reconfiguration," *IEEE Transactions on Industrial Informatics*, vol. 15, no. 10, pp. 5444-5455, Feb. 2019.

[9] Y. Li, W. Sun, W. Yin *et al*., "Restoration strategy for active distribution systems considering endogenous uncertainty in cold load pickup," *IEEE Transactions on Smart Grid*, vol. 13, no. 4, pp. 2690-2702, Jul. 2022.

[10] Y. Deng, W. Jiang, F. Hu *et al*., "Resilience-oriented dynamic distribution network with considering recovery ability of distributed resources," *IEEE Journal on Emerging and Selected Topics in Circuits and Systems*, vol. 12, no. 1, pp. 149-160, Mar. 2022.

[11] D. N. Trakas and N. D. Hatziargyriou, "Optimal distribution system operation for enhancing resilience against wildfires," *IEEE Transactions on Power Systems*, vol. 33, no. 2, pp. 2260-2271, Mar. 2018.

[12] L. Che and M. Shahidehpour, "Adaptive formation of microgrids with mobile emergency resources for critical service restoration in extreme conditions," *IEEE Transactions on Power Systems*, vol. 34, no. 1, pp. 742-753, Jan. 2019.

[13] B. Chen, C. Chen, J. Wang *et al*., "Sequential service restoration for unbalanced distribution systems and microgrids," *IEEE Transactions on Power Systems*, vol. 33, no. 2, pp. 1507-1520, Mar. 2018.

[14] A. Arif, S. Ma, Z. Wang *et al*., "Optimizing service restoration in distribution systems with uncertain repair time and demand," *IEEE Transactions on Power Systems*, vol. 33, no. 6, pp. 6828-6838, Jul. 2018.

[15] H. Wu, Y. Xie, Y. Xu *et al*., "Robust coordination of repair and dispatch resources for post-disaster service restoration of the distribution system," *International Journal of Electrical Power & Energy Systems*, vol. 136, p. 107611, Mar. 2022.

[16] X. Yang, C. Xu, J. Wen *et al*., "Cooperative repair scheduling and service restoration for distribution systems with soft open points," *IEEE Transactions on Smart Grid*, vol. 14, no. 3, pp. 1827-1842, May 2023.

[17] J. Najafi, A. Anvari-Moghaddam, M. Mehrzadi *et al*., "An efficient framework for improving microgrid resilience against islanding with battery swapping stations," *IEEE Access*, vol. 9, pp. 40008-40018, Jan. 2021.

[18] Q. Sui, F. Li, C. Wu *et al*., "Optimal scheduling of battery charging-swapping systems for distribution network resilience enhancement," *Energy Reports*, vol. 8, pp. 6161-6170, Nov. 2022.

[19] Y. Guo, K. Liao, J. Yang *et al*., "Service restoration for resilient distribution system with coordination of battery swapping stations and distributed generations," *IET Renewable Power Generation*, vol. 17, no. 4, pp. 814-828, Nov. 2022.

[20] X. Zhao, Y. Yang, M. Qin *et al*., "Day-ahead dispatch of novel battery charging and swapping station based on distributionally robust optimization," *Journal of Energy Storage*, vol. 63, p. 107080, Jul. 2023.

[21] T. Ding, Z. Wang, W. Jia *et al*., "Multiperiod distribution system restoration with routing repair crews, mobile electric vehicles, and soft-open-point networked microgrids," *IEEE Transactions on Smart Grid*, vol. 11, no. 6, pp. 4795-4808, Nov. 2020.

[22] J. Li, M. E. Khodayar, and M. R. Feizi, "Hybrid modeling based co-optimization of crew dispatch and distribution system restoration considering multiple uncertainties," *IEEE Systems Journal*, vol. 16, no. 1, pp. 1278-1288, Mar. 2022.

[23] Y. Zhou, M. Shahidehpour, Z. Wei *et al*., "Distributionally robust unit commitment in coordinated electricity and district heating networks," *IEEE Transactions on Power Systems*, vol. 35, no. 3, pp. 2155-2166, May 2020.

[24] R. Leng, Z. Li, and Y. Xu, "Two-stage stochastic programming for coordinated operation of distributed energy resources in unbalanced active distribution networks with diverse correlated uncertainties," *Journal of Modern Power Systems and Clean Energy*, vol. 11, no. 1, pp. 120-131, Jan. 2023.

[25] D. Yu, G. Liu, M. Guo *et al*., "An improved *K*-medoids algorithm

based on step increasing and optimizing medoids," *Expert Systems with Applications*, vol. 92, pp. 464-473, Feb. 2018.
[26] Y. Zou, Y. Xu, and C. Zhang, "A risk-averse adaptive stochastic optimization method for transactive energy management of a multi-energy microgrid," *IEEE Transactions on Sustainable Energy*, vol. 14, no. 3, pp. 1599-1611, Jul. 2023.
[27] S. Chen, Y. Yang, M. Qin *et al*., "Coordinated multiobjective optimization of the integrated energy distribution system considering network reconfiguration and the impact of price fluctuation in the gas market," *International Journal of Electrical Power & Energy Systems*, vol. 138, p. 107776, Jun. 2022.
[28] M. E. Baran and F. Wu, "Network refiguration in distribution system for loss reduction and load balancing," *IEEE Transactions on Power Delivery*, vol. 4, no. 2, pp. 1401-1407, Apr. 1989.
[29] J. S. Savier and D. Das, "Impact of network reconfiguration on distribution systems performance," *IEEE Transactions on Power Delivery*, vol. 22, no. 4, pp. 2473-2480, Oct. 2007.

Xianqiu Zhao received the B.E. degree in electrical engineering from Hohai University, Nanjing, China, in 2017, and the M.E. degree in electrical engineering from North China Electric Power University, Beijing, China, in 2020. He is currently pursuing the Ph.D. degree in electrical engineering from Southeast University, Nanjing, China. His research interests include renewable energy and electric vehicle.

Qingshan Xu received the B.E. degree from Southeast University, Nanjing, China, in 2000, the M.E. degree from Hohai University, Nanjing, China, in 2003, and the Ph.D. degree from Southeast University, in 2006, all in electrical engineering. From 2007 to 2008, he was a Visiting Scholar and cooperated with the Aichi Institute of Technology, Toyota, Japan. He is currently a Full Professor with school of Electrical Engineering, Southeast University. His research interests include renewable energy, power system operation and control.

Yongbiao Yang received the B.E. degree in electrical engineering from Southwest Jiaotong University, Chengdu, China, in 2001, and the M.E. degree in energy and power engineering from Nanjing University of Science and Technology, Nanjing, China, in 2013. He is currently a Senior Engineer at Southeast University, Nanjing, China. His research interests include reliability analysis, demand response, and integrated energy system.